Available online at www.eccomasproceedia.org
Eccomas Proceedia COMPDYN (2025) 605-615

ECCOMAS
Proceedia

COMPDYN 2025
10th ECCOMAS Thematic Conference on
Computational Methods in Structural Dynamics and Earthquake Engineering
M. Papadrakakis, M. Fragiadakis (eds.)
Rhodes Island, Greece, 15-18 June 2025

DYNAMIC RESPONSE HISTORY ANALYSIS AND STRUCTURAL SYSTEM IDENTIFICATION OF A LARGE-SCALE INTEGRATED TRANSPORTATION HUB

Yong Yuan[1, 2] **and Zhi-Han Zhang**[2]

[1] State-key Laboratory of Disaster Reduction in Civil Engineering
Shanghai China
yuany@tongji.edu.cn

[2] College of Civil Engineering, Tongji University
Shanghai China
2410078@tongji.edu.cn

Abstract

Comprehensive transportation hubs combine both underground and aboveground components, which would exhibit complex dynamic characteristics under seismic excitations due to their integrated structural configuration. To study the dynamic response characteristics of the combined aboveground-underground structures, dynamic response history analysis is performed on a 4-story, 12-span integrated structure accounting for soil-structure interaction. Based on the response history data, the natural frequencies and deformation mode shapes of the combined structure system are identified using eigensystem realization algorithm. Furthermore, the seismic response of a 2-story single underground structure is compared with that of the 4-story combined structure to investigate the integrated interactions among ground, underground structures and aboveground structures. From the identified modes of the combined structure system, a phase difference between the motions of aboveground and underground structure is observed when comparing the lower-order and higher-order deformation modes. Additionally, the response history results indicate that the presence of the combined aboveground structure amplifies the inertial effects, yielding a more pronounced spatial distribution of drift ratios and internal forces in the underground story directly connected to the aboveground structure. However, the amplification effects decrease sharply with increasing depth. The insights into the deformation modes and the force distribution are expected to inform significantly the seismic design of comprehensive transportation hubs.

Keywords: Transportation Hubs, Integrated Aboveground-Underground Structure, System Identification, Response History Analysis, Structural Vibration Mode.

ISSN:2623-3347
Peer-review under responsibility of the organizing committee of COMPDYN 2025.
doi: 10.7712/120125.12433.25867

1 INTRODUCTION

As key components of the development concept of "station-city integration", comprehensive transportation hubs represent a significant innovation in modern urban infrastructure construction. To achieve effective integration of transportation and urban functions, underground structures (such as shopping malls and metro stations) are directly connected to the aboveground structures (such as airport terminals and transit centers) in the transportation hubs, forming a large-scale integrated aboveground-underground structure system. Extensive research has been conducted on the seismic performance of individual aboveground or underground structures, including airport terminals[1], metro stations[2, 3], and tunnels[4]. However, due to the oscillation of the aboveground structures, the overall seismic response of integrated aboveground-underground structures is quite distinct from that of isolated underground structures [5]. The structural dynamic characteristics of the integrated structures still requires further investigation.

In this study, three-dimensional finite element analysis was conducted on an integrated aboveground-underground structure, and a single underground structure was also simulated for comparison. Based on the dynamic response histories, the structural natural frequencies and deformation modes were identified using an eigensystem realization algorithm, and the identified results were validated in the frequency domain. Furthermore, through response history analysis, this study also systematically investigated the effects of the combined aboveground structure on the inter-story racking deformation and dynamic internal forces of the underground structure.

2 PROBLEM STATEMENT

This paper investigates the dynamic response characteristics of an integrated aboveground-underground structure using a 4-story, 12-span model (Model A), with dimensions of 108 m × 108 m × 24 m (length × width × height). The integrated aboveground-underground comprises two underground stories and two integrated aboveground stories. This configuration is idealized based on a comprehensive transportation hub under construction. To evaluate the influence of the presence of aboveground component, a single underground structure model is also employed in the research. The single underground structure (Model B), is 108 m × 108 m × 12 m (length × width × height) with 12 spans and 2 underground stories in cross-section. In each model, the scales of a span and a story are 9 m and 6 m, respectively. The columns are 1.2 m × 1.2 m and beams are 0.6 m × 1.2 m (width × height). The thicknesses of slabs, walls and baseplate are 0.2m, 0.8m and 1.0m, respectively. The concrete materials used for different structural components are listed in Table 1. For the sake of simplicity, the soil deposit is idealized as one homogeneous layer, whose material properties are selected by the actual site conditions, with density of 2000 kg/m3, Young's modulus of 480MPa, and Poisson's ratio of 0.28.

Materials	**Structural Components**	**Density** (kg/m^3)	**Young's Modulus** (MPa)	**Poisson's Ratio** $(-)$
C40	Columns, Beams	2450	3.25×10^4	0.2
C45	Slabs, Walls	2450	3.35×10^4	0.2

Table 1: Properties of the concrete material

The finite element simulation was conducted using the widely used program ABAQUS. In finite element models, the beams and columns of the structures were simulated by the beam element B31 while the slabs, walls, and baseplates were meshed by the shell element S4R. The soil was discretized with the solid element C3D8R. The element size for the structural components was set to 1.5m. For the model soil, the element size was limited to less than one-tenth of the shear wave's wavelength, so as to ensure accurate reproduction of the input waveforms. The finite element models of the soil-structure systems are shown in Fig. 1.

Kinematic tie constraints were applied to simulate the lateral free-field conditions at the side boundaries, where the horizontal motion of the boundary nodes at the corresponding heights is constrained to be the same. The three-dimensional viscous-elastic artificial boundary and the according wave input method were employed in this study. By introducing the springs and dashpots, the base boundary was simulated as the elastic bedrock. According to [6], the coefficients of springs and dashpots are as follows:

In the normal direction

$$K_n = \alpha_n G/R ; \quad C_n = \rho c_p \tag{1}$$

In the tangential direction

$$K_\tau = \alpha_\tau G/R ; \quad C_\tau = \rho c_s \tag{2}$$

where K_n and C_n are the coefficients of springs and dashpots in the normal direction; K_τ and C_τ are the coefficients of springs and dashpots in the tangential direction; R is the distance between the wave source and the artificial boundary; G is the shear modulus and ρ is the density of the soil; c_p and c_s are the propagation velocities of the compression waves and shear waves in the medium, respectively.

The seismic input wave was selected as an artificial rock motion record generated based on a 10% exceedance probability in 100 years for the construction site. The time history and Fourier spectrum of the input motion are shown in Fig. 2. The selected seismic wave has a duration of 60 seconds and a peak acceleration (PA) of 0.24g. Additionally, to determine the natural frequency of the structure, a white noise sweep with a PA of 0.1g was also applied.

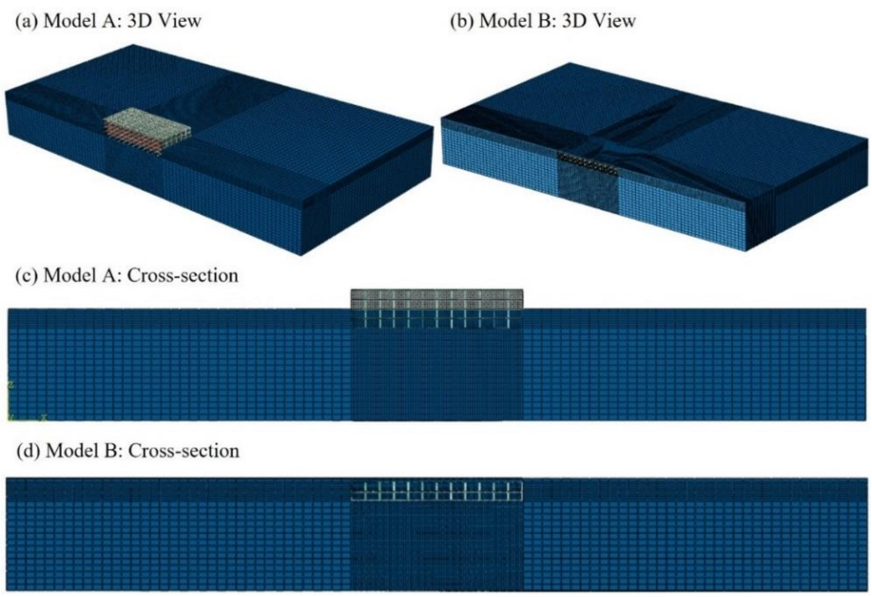

Figure 1: Finite element models

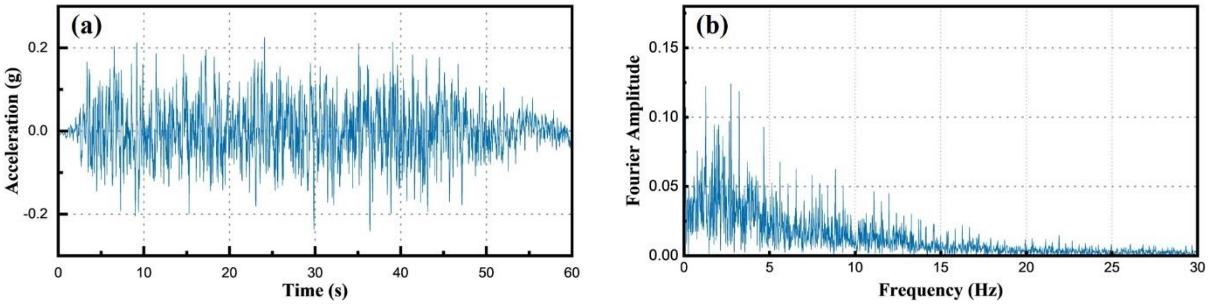

Figure 2: Seismic record of artificial rock motion: (a) time history and (b) Fourier spectrum

3 SYSTEM IDENTIFICATION FROM TIME HISTORY RESPONSE

In this section, a system identification method based on dynamic response histories is developed. Firstly, the input and output matrices are constructed based on the dynamic response histories of the integrated structure, and the system's Markov parameters are computed accordingly. Secondly, an eigensystem realization algorithm[7] is employed to reconstruct the dynamic system matrices, from which the modal parameters can be finally identified.

3.1 Model in discrete time space

For a discrete-time, linear, dynamical system with n degrees-of-freedom, the state-space model can be expressed as :

$$\begin{cases} x(k+1) = Ax(k) + Bu(k) \\ y(k) = Cx(k) \end{cases} \tag{3}$$

where integer k is the discrete-time indicator, $x(k) \in R^{N\times 1}$ is the state vector, $u(k) \in R^{m\times 1}$ is the control input vector, $y(k) \in R^{p\times 1}$ is the output/measurement vector, $A \in R^{N\times N}$ is the system matrix which characterizes the dynamics of the system, $B \in R^{N\times m}$ is the input matrix, $C \in R^{p\times N}$ is the output matrix, $N(=2n)$ is the system order, m is the dimension of input vectors, and p is the number of output channels.

With the assumption of zero initial conditions, the set of this equations for a sequence of l can be written as:

$$y = YU \tag{4}$$

where

$$y = \begin{bmatrix} y(1) & y(2) & \cdots & y(l) \end{bmatrix} \tag{5}$$

$$Y = \begin{bmatrix} CB & CAB & \cdots & CA^{l-1}B \end{bmatrix} \tag{6}$$

and

$$U = \begin{bmatrix} u(0) & u(1) & \cdots & u(l-1) \\ & u(0) & \cdots & u(l-2) \\ & & \ddots & \vdots \\ & & & u(0) \end{bmatrix} \tag{7}$$

By solving Y from the Eq. (4), the time domain representation of the relationship between input and output histories, also known as the Markov parameters, can be obtained as:

$$Y(k) = CA^{k-1}B \tag{8}$$

3.2 Eigensystem realization

To solve the system matrices $[A, B, C]$, the Markov parameters in Eq. (8) are built into the $r \times s$ block matrix (generalized Hankel matrix):

$$\begin{aligned} H(k) &= \begin{bmatrix} Y(k+1) & Y(k+2) & \cdots & Y(k+s) \\ Y(k+2) & Y(k+3) & \cdots & Y(k+2+s) \\ \cdots & \cdots & \cdots & \cdots \\ Y(k+r) & Y(k+r+1) & \cdots & Y(k+r+s-1) \end{bmatrix} \\ &= \begin{bmatrix} C \\ CA \\ \cdots \\ CA^{r-1} \end{bmatrix} A^k \begin{bmatrix} B & AB & \cdots & A^{s-1}B \end{bmatrix} = V_r A^k W_s \end{aligned} \tag{9}$$

where V_r and W_s are the observability and controllability matrices, and the parameter r and s are the observability and the controllability indices, respectively.

Then conduct the singular value decomposition for $H(k)$ with $k = 0$:

$$H(0) = PDQ^T \tag{10}$$

Where $P \in R^{rp \times N}$ and $Q \in R^{sm \times N}$ are the decomposed left and right matrices, respectively. Define 0_p as a null matrix of order p, I_p an identity matrix, $E_p^T = [I_p,\ 0_p, \ldots, 0_p]$, $E_m^T = [I_m,\ 0_m, \ldots, 0_m]$, the system matrices can be obtained as:

$$A = D^{-1/2} P^T H(1) Q D^{-1/2} \tag{11}$$

$$B = D^{1/2} Q^T E_m \tag{12}$$

$$C = E_p^T P D^{1/2} \tag{13}$$

3.3 Determination of modal parameters

After constructing system matrices $[A, B, C]$ using the ERA method, by performing the eigenvalue decomposition of A, we can obtain the eigenvalues λ and eigenvectors ψ such that:

$$\psi_i^{-1} A \psi_i = \lambda_i \tag{14}$$

From Eq. (14), the natural frequency and damping ratio of the system can be obtained as:

$$f_i = \frac{|f_s \ln \lambda_i|}{2\pi}; \ \zeta_i = -\frac{(\ln \lambda_i)^R}{|\ln \lambda_i|} \tag{15}$$

where f_s is the sampling frequency. || is the complex modulus.

And the modal shape vector can be obtained as:

$$\phi_i = C\psi_i \tag{16}$$

4 RESULTS

In this section, the seismic responses of the models are compared, regarding the structural racking deformation and the column's bending moments. Since the horizontal seismic wave propagates in the X direction in the simulation, a representative framework located in the center along the Y-axis is selected as the key analysis section for both models. The columns of this framework are sequentially numbered from left to right as Col.1- Col.13. From the bottom to the top, the four stories of the integrated aboveground-underground structures are numbered as B2, B1, F1, and F2.

4.1 Structural racking deformation mode

During earthquakes, underground structures undergo racking deformation under the action of soil shear deformation. In this section, the deformation modes of the integrated aboveground–underground structure (Model A) are identified based on the dynamic response histories recorded at the frame column ends. To expedite the computational process, only the deformation modes of the left half of the structure (Col.1– Col.7) are directly identified, with the corresponding modes for the right half (Col.8– Col.13) assumed to be symmetric.

In Model A, displacement response histories at the column ends are extracted from the FE models, and at the k^{th} time increment, the displacement responses are assembled into a 35-dimensional output vector, $y(k)$. Concurrently, the earthquake excitation at the k^{th} time increment is represented by a one-dimensional input vector, $u(k)$. The system modal identification method, described in the previous section, is then applied to analyze the deformation modes. The analysis results are summarized in Table 2.

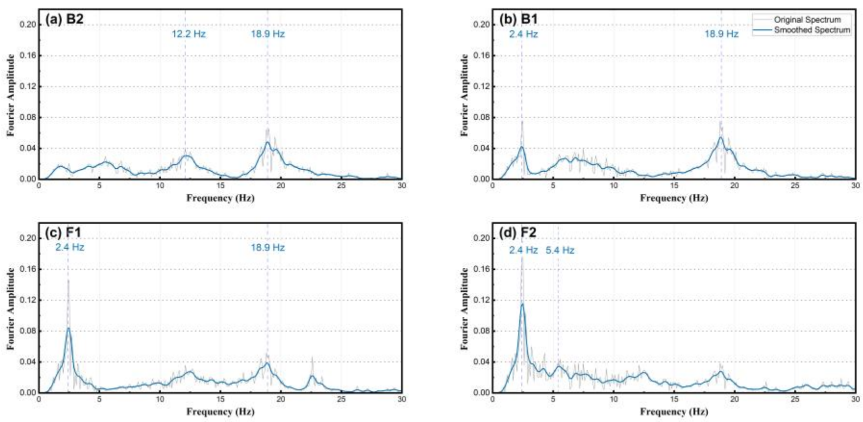

Figure 3: Fourier spectra of acceleration responses on: (a) B2, (b) B1, (c) F1, and (d) F2

The identified modal frequencies of Model A were 2.33 Hz, 5.23 Hz, 11.9 Hz, and 18.9 Hz, respectively. To validate the accuracy of the identification results, white noise excitation was applied to Model A. The Fourier spectra of the dynamic responses at the frame column ends on each floor are presented in Fig. 3. Within the frequency range considered in the numerical simulation (0–50 Hz), the first four natural frequencies can be identified from these spectra, and the dominant frequency components of the structural response are consistent with the identified deformation mode frequencies. However, the amplitude in the Fourier spectra indicates the predominant frequency components differ significantly between the underground and aboveground structures. As shown in Fig. 3(a), the spectrum of the underground structure's dynamic response exhibits significant amplitude peaks near 12.2 Hz and 18.9 Hz, indicating that the response of the underground component is primarily governed by higher-order modes. In contrast, for the aboveground structure (Fig. 3(c)-(d)), the 2.5 Hz mode is the principal contributor to the dynamic response of the F1 and F2 floors, as it dominates the Fourier amplitude spectrum.

No.	Frequency(Hz)	Displacement Mode Shapes							
1	2.33		**Col.1**	**Col.2**	**Col.3**	**Col.4**	**Col.5**	**Col.6**	**Col.7**
		F2	6.45	6.45	6.45	6.45	6.45	6.45	6.45
		F1	4.24	4.24	4.24	4.25	4.26	4.26	4.26
		B1	1.09	1.21	1.30	1.37	1.41	1.43	1.44
		B2	-0.51	-0.50	-0.48	-0.47	-0.46	-0.45	-0.45
		Base	-1.25	-1.31	-1.35	-1.37	-1.37	-1.36	-1.36
2	5.23		**Col.1**	**Col.2**	**Col.3**	**Col.4**	**Col.5**	**Col.6**	**Col.7**
		F2	-5.60	-5.60	-5.60	-5.60	-5.65	-5.65	-5.65
		F1	-0.14	-0.15	-0.16	-0.17	-0.18	-0.19	-0.19
		B1	3.69	3.60	3.53	3.47	3.43	3.41	3.40
		B2	4.22	4.23	4.24	4.24	4.25	4.25	4.25
		Base	2.50	2.50	2.53	2.54	2.55	2.59	2.61
3	11.9		**Col.1**	**Col.2**	**Col.3**	**Col.4**	**Col.5**	**Col.6**	**Col.7**
		F2	0.99	0.99	0.98	0.98	0.97	0.97	0.97
		F1	-0.79	-0.79	-0.79	-0.79	-0.79	-0.79	-0.79
		B1	-1.46	-1.46	-1.44	-1.41	-1.39	-1.38	-1.37
		B2	1.28	1.45	1.62	1.76	1.86	1.93	1.95
		Base	1.94	2.00	2.09	2.17	2.23	2.26	2.27
4	18.9		**Col.1**	**Col.2**	**Col.3**	**Col.4**	**Col.5**	**Col.6**	**Col.7**
		F2	-1.07	-1.11	-1.14	-1.16	-1.18	-1.19	-1.19
		F1	1.74	1.75	1.75	1.73	1.71	1.70	1.69
		B1	-1.71	-1.80	-1.88	-1.95	-1.99	-2.02	-2.03
		B2	1.22	1.39	1.55	1.69	1.81	1.88	1.91
		Base	-0.48	-0.50	-0.47	-0.42	-0.38	-0.35	-0.34

Table 2: Identified modal parameters of Model A

Fig. 4 illustrates the raking deformation mode shapes of Model A corresponding to the identified results in Table 2. In Fig. 4, gray lines denote the undeformed frame structure, colored lines denote the deformed frame structure, and gray blocks represent the surrounding ground.

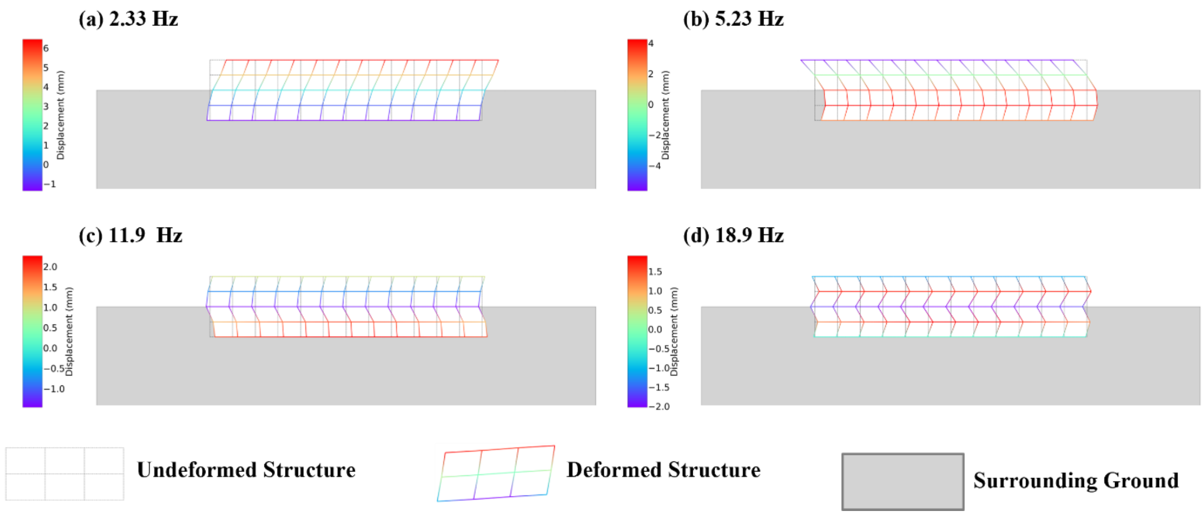

Figure 4: Identified racking deformation modes of Model A

From the identified mode shapes, it can be observed that the phase difference between the motions of the aboveground and underground components determines the characteristics of the structural response. In the lower-order modes (see Fig. 4(a)-(b)), the motion of aboveground structure is in consistent with that of underground structure, whereas in the higher-order modes (see Fig. 4(c)-4(d)), the motion of the aboveground structure is opposite to that of underground structure.

4.2 Structural inter-story drift ratio

The displacement difference between the top and the bottom of the columns is widely used to assess the structural vulnerability. Both in Model A and Model B, the peak values of the inter-story drift ratio are compared in Fig. 5.

It can be observed from the Fig. 5(a) that in the integrated aboveground-underground structure, the maximum inter-story drift ratio occurs on the F1 floor, with a peak drift angle of 1/543. In the underground component, the maximum inter-story drift ratios for the B2 and B1 stories are 1/1096 and 1/759, respectively. This indicates that the floors directly connected to the aboveground structure experience the greatest raking deformation under seismic loading. Furthermore, within the same underground floor, the drift ratios of the frame columns gradually increase from the sides toward the center, exhibiting an “arch-shaped” distribution. This behavior is attributed to the diminishing lateral confinement provided by the surrounding soil from the edges toward the center, resulting in more pronounced drift ratios in the central frame columns.

In Fig. 5(b), the inter-story drift ratio at B1 story in Model A is significantly higher than that in Model B, indicating that the aboveground structure amplifies the shear deformation of the underground structure. To quantify the influence of aboveground component on the underground structure’s racking deformation, the relative difference in the drift ratio at B1 and B2 floor, denoted as γ_D, is compared in Table 3. γ_D is calculated in the form of Eq. (17).

$$\gamma_D = (D_I - D_U) / D_U \times 100\% \tag{17}$$

where D_I and D_U are the drift ratios in Model A and Model B, respectively. Table 3 shows that the underground structure’s drift ratio at B1 story is increased by 46.5%- 57.8%, whereas at B2 story, the drift ratio is mitigated due to the presence of aboveground structure.

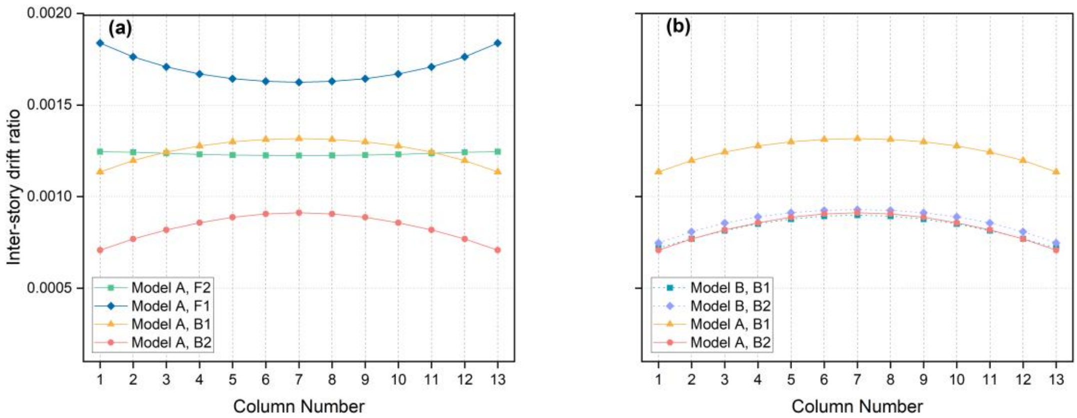

Figure 5: Distribution of drift ratio of (a) B2-F2 in Model A, (b) B2-B1 in Model A and Model B

γ_D (%)	Col.1	Col.2	Col.3	Col.4	Col.5	Col.6	Col.7	Col.8	Col.9	Col.10	Col.11	Col.12	Col.13
B1	57.8	55.5	52.6	49.9	48.0	46.9	46.5	46.9	48.0	49.9	52.6	55.5	57.8
B2	-5.3	-5.0	-4.4	-3.6	-2.7	-2.1	-1.9	-2.1	-2.7	-3.6	-4.4	-5.0	-5.3

Table 3: Distribution of relative difference in drift ratio between Model A and Model B

4.3 Structural inter-story drift ratio

For underground structures, frame columns are considered important load bearing components, which are also most susceptible to seismic damages. This study examines the influence of the aboveground structure on the underground structure's internal forces, regarding the peak bending moment. The relative differences in the internal forces between the two models are analyzed to quantitatively assess the amplifying effect of the aboveground structure on the internal forces of the underground structure. The relative differences in bending moment, denoted as γ_M , are calculated in Eq. (18) and compared in Fig. 6.

$$\gamma_M = (M_I - M_U) / M_U \times 100\% \tag{18}$$

where M_I and M_U are the bending moments in model A and Model B, respectively.

A positive γ_M indicates that the presence of aboveground structure amplifies the bending moment response of the frame columns in the underground structure, whereas a negative γ_M indicates that the aboveground structure mitigates the underground structure's response. In Fig. 6, the maximum value of γ_M is 74.3% and occurs at the column top at the B1 story, which is directly connected to the aboveground structure. As the depth increases, γ_M gradually decreases and becomes negative at the bottom columns in the B2 level. This finding demonstrates that the presence of the aboveground structure directly amplifies the bending moments in the connected underground frame columns, while also reducing the bending moments at the base of the columns in the lower underground level.

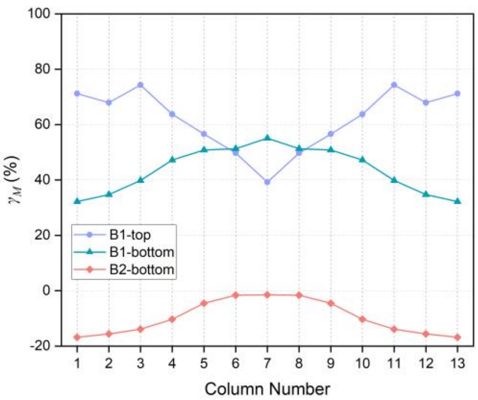

Figure 6: Distribution of relative difference in bending moment between Model A and Model B

5 CONCLUSIONS

In this study, a series of three-dimensional finite element dynamic response history analysis were conducted, and a system identification method based on dynamic response histories was developed to investigate the racking deformation modes of an integrated aboveground-underground structure. The first four racking deformation modes were identified for the 4-story integrated structure. Additionally, to assess the influence of the aboveground structure on the seismic response of the connected underground structure, the racking deformation and internal forces of the integrated aboveground-underground structure were compared with those of a single underground structure.

The following conclusions were drawn for the integrated aboveground-underground structure:

- The identified natural frequencies compare adequately well with the dominant frequency components in the Fourier spectra, with relative error of less than 3%. According to the amplitude of the Fourier spectra, the dynamic response of the aboveground component within the integrated aboveground-underground structure is governed by the lower-order deformation modes, whereas the underground component is more influenced by the higher-order modes.

- A phase difference between the motions of aboveground and underground structures can be observed through the identified racking deformation modes. The motion of aboveground structure is in consistent with that of underground structure in the lower-order modes, while opposite to that of underground structure in higher-order modes.

- The presence of aboveground structure significantly increases the racking deformation and internal forces within the underground structure. Specifically, the B1 story, which is directly connected to the aboveground structure, suffers the most intense amplification, with a 57.8% increase in inter-story drift ratios and a 74.3% increase in bending moments. However, the influence of aboveground structures diminishes with increasing depth. In the B2 story, the drift ratios are mitigated by the presence of aboveground structure, and the peak bending moments at the column bases are reduced by 1.5%-15.6% in the integrated aboveground-underground system.

REFERENCES

[1] Cucuzza, R., Aloisio, A., Domaneschi, M. et al, Multimodal seismic assessment of infrastructures retrofitted with exoskeletons: insights from the Foggia Airport case study. *Bulletin of Earthquake Engineering*, 22, 3323–3351, 2024.

[2] Wu W, Ge S, Yuan Y, et al, Seismic response of subway station in soft soil: Shaking table testing versus numerical analysis. *Tunnelling and Underground Space Technology*, 100, 103389, 2020.

[3] Cai X, Yang C, Liu Z, Jiang L, Yuan Y, Effects of axial compression ratio on seismic behavior of shallow-buried rectangular stations: Hybrid simulation and quasi-static test. *Earthquake Engineering & Structural Dynamics*, 53, 2734–2755, 2024.

[4] Yuan Y, Wang Q, Liu T, Yu H, Anastasopoulos I, Seismic response of ground penetrating shield tunnels under lateral harmonic excitations: insights from shaking table test. Earthquake Engineering & Structural Dynamics 54, 867–884, 2025.

[5] Li W-T, Wang R, Zhang J-M, Influence of aboveground structure on connected underground structure seismic response within an integrated system. *Tunnelling and Underground Space Technology*, 134, 105003, 2023.

[6] Liu J, Du Y, Du X, Wang Z, Wu J, 3D viscous-spring artificial boundary in time domain. *Earthquake Engineering and Engineering Vibration*, 5, 93–102, 2006.

[7] Juang J-N, Pappa RS, An eigensystem realization algorithm for modal parameter identification and model reduction. *Journal of Guidance, Control, and Dynamics*, 8:5, 620-627, 1985.